Available online at www.sciencedirect.com

ScienceDirect

Procedia Materials Science 8 (2015) 1004 – 1013

Procedia Materials Science

www.elsevier.com/locate/procedia

International Congress of Science and Technology of Metallurgy and Materials, SAM - CONAMET 2013

Application of the LIBS Technique to the Study of Fast Impurities Diffusion in Zr Based Alloys

C. Ararat-Ibarguen[a,b]*, C. Corvalán[b,c,d], N.Di Lalla[c], M. Iribarren[a,b], R. Pérez[a,b,c] and E. Vicente[a,b]

[a]*Instituto Sabato (UNSAM-CNEA), Buenos Aires, Argentina.*
[b]*Gerencia Materiales, CAC, CNEA, Av. del Libertador 8250, (C1429BNP) BuenosAires,Argentina*
[c]*Consejo Nacional de Investigaciones Científicas y Técnicas,Argentina.*
[d]*Universidad Nacional de Tres de Febrero (UNTREF), Argentina.*

Abstract

The following paper presents a significant advance in the study of the interdiffusion between Zr-2.5wt%Nb and ASTM 410 martensitic grade stainless steel by means of LIBS (Laser Induced Breakdown Spectroscopy) technique. Both materials are very important in the nuclear industry. Interdiffusion profiles show a slow diffusion of Zr and Nb in the steel matrix, as well as a fast diffusion of Fe, C and Cr in the matrix of the Zr-base alloy. Also, the formation of intermetallic phases was observed by scanning electron microscopy. In addition, diffusivity values of Cr and Fe in the Zr-based alloy were determined at 900ºC.

Selection and peer-review under responsibility of the scientific committee of SAM - CONAMET 2013

Keywords: LIBS, diffusion, nuclear materials

1. Introduction and purposes

Laser-induced Breakdown Spectroscopy (LIBS) is an atomic emission spectroscopy technique that employs high density energy lasers as the excitation source. It detects, and eventually determines, the atomic composition. No

* Corresponding author. Tel.: +54-11-6772-7748; fax: +54-11-6772-7763.
E-mail address: ibarguren@cnea.gov.ar

Selection and peer-review under responsibility of the scientific committee of SAM - CONAMET 2013
doi:10.1016/j.mspro.2015.04.162

sample preparation is needed and its resolution involves a few ppm (Lee et al. 2001). The laser pulse produces ablation of a fraction of the material and in the subsequent cooling time, the plasma produces both continuous and discrete emissions which are collected by a spectrometer providing the corresponding emission spectra of the sample (Mizlolek et al. 2008). In the present case, and as an application to solid state diffusion studies, we present the results of the analysis of the interdiffusion zone between martensitic stainless steels ASTM type 410 and Zr-2.5wt%Nb (Zr-2.5Nb) alloy, (CANDU type reactors material). Concentration profiles of Zr, Nb, Fe, Ni and Cr between 600 and 900 °C were obtained. Microstructural characterization was carried out by optical and scanning electron microscopy (SEM) of the diffusion couples. Finally, experiments involving infinite dilution diffusion were performed in order to obtain the true diffusion coefficients of Fe and Cr in Zr-2.5Nb at 900 °C.

2. Experimental procedure

The Zr-2.5Nb alloy (ATI Wah Chang, ASTM B 353-02 - R60901), Fig. 1a, shows very fine grains of α-Zr phase surrounded by a thin layer of β-Nb, oriented in the longitudinal direction of the pressure tube. Stainless steel ASTM 410,, was used instead of the ASTM 403,martensitic grade, usually employed in the "End Fitting" nuclear reactor fuel elements. In Fig. 1b, it can be seen both martensitic-ferritic needle type grains as well as phase segregation by incomplete transformation of the material (Metals Handbook, 1985). The chemical composition of both alloys can be seen in Table 1.

Table 1. Chemical composition of the alloys Zr-2.5Nb and stainless steel ASTM 410 martensitic grade.

Zr-2.5Nb	**Nb (%)**	**O (%)**	**Al (ppm)**	**Fe (ppm)**	**Cr (ppm)**	**Ti (ppm)**	**U (ppm)**
	2.4-2.8	0.09-0.13	75	1500	200	50	3.5
	C (%)	**Cr (%)**	**Ni (%)**	**Si (%)**	**P (%)**	**S (%)**	
ASTM 410	0.15	11.5	0.75	1.0	0.04	0.03	

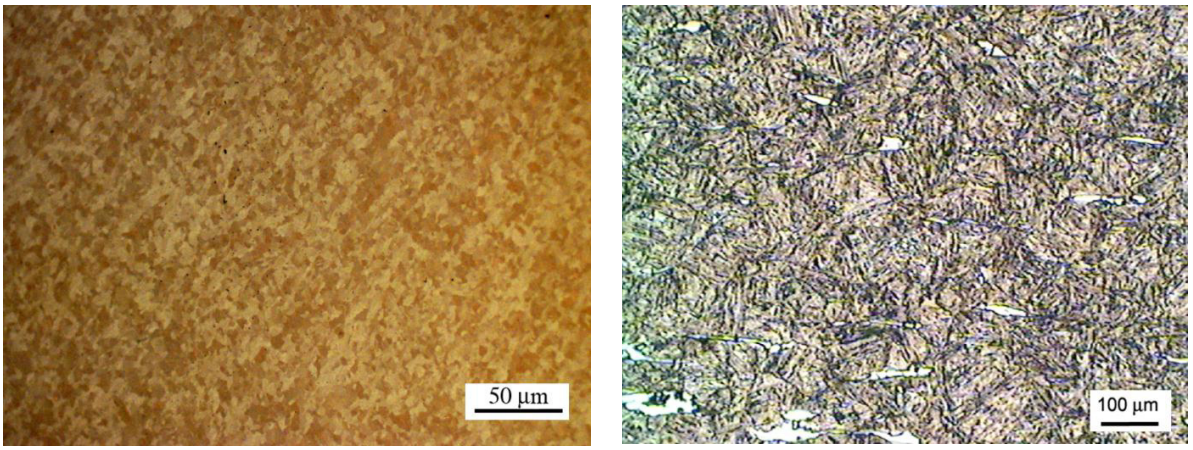

Fig. 1. Optical micrographs of: (a) Alloy Zr-2.5Nb, polarized light;(b) ASTM 410 steel, martensitic grade.

Diffusion couples were prepared from (0.5 x 1.0 x 0.3) cm plates. They were mirror polished up to 1 µm with diamond paste in the case of the steel, and with potassium dichromate and 0.05% HF in aqueous solution in the case of the Zr alloy. For a proper adhesion of the materials constituting the pair of diffusion, they were placed in an ad-hoc press device with a constant pressure of 5 to 10 MPa. This assembly was annealed in an oven at 900 °C in dynamic vacuum better than 8 10^{-6} mbar for 3 h (Ararat, 2013). Samples for infinite dilution diffusion experiments were prepared with two $FeCl_3$ and $Cr(NO_3)_3$ aqueous solutions drops onto the polished Zr-2.5Nb samples and then dried with an IR lamp. Different heat treatments (from 3 to 123 h) and 600, 700, 800 and 900 °C were performed with slow cooling for the diffusion couples in order to avoid embrittlement of the junction. In the case of diffusion at

infinite dilution, the samples were annealed at 900 °C for 1 h for Fe diffusion, and 4 h for the diffusion of Cr. Finally, in both case they were quenched in cold water.

A LIBS equipment, namely a 2500+ Ocean Optics model, Fig. 2, (50 mJ, 200-500 nm wavelength range) was used. To obtain the interdifusión profiles of the diffusion couples, laser scanning processes from one material to the other were performed with a 50-100 μm step, Fig. 3a. For the infinite dilution experiments, the Cr profiles measurements were performed parallel to the diffusion direction (left side of Fig. 3b), while perpendicular measurements were preferred to the Fe experiments. In all the cases the energy of the laser source used was 4.53 J (98% of the maximum power of the laser). Both interdiffusion and diffusion at infinite dilution profiles were obtained after monitoring different emission lines of a given element. The value of the relative signal intensity is given by equation (1).

$$I_{relativeintensity} = \frac{A(x)}{A(T)}\Lambda \tag{1}$$

Where: *A(x)* is the area of the signal corresponding to the emission line of the element of interest, A*(T)* is the total area of the spectrum and Λ is a numerical factor. Table 2 showsthe emission lines selected in this work.

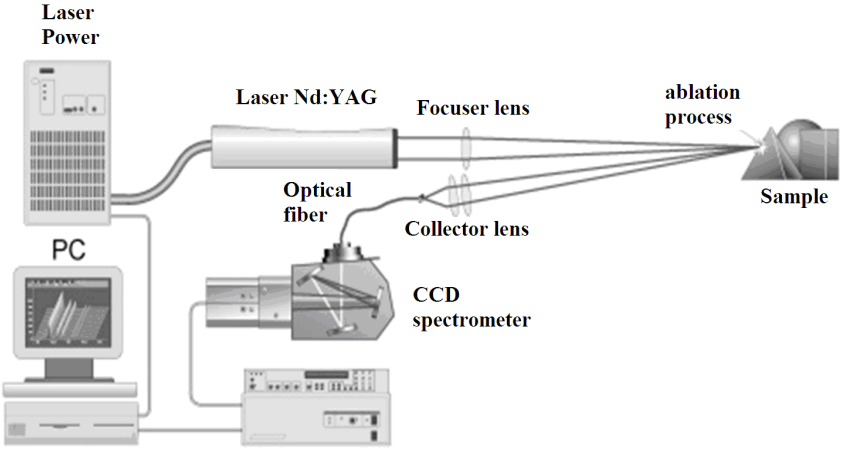

Fig. 2. LIBS equipment diagram.

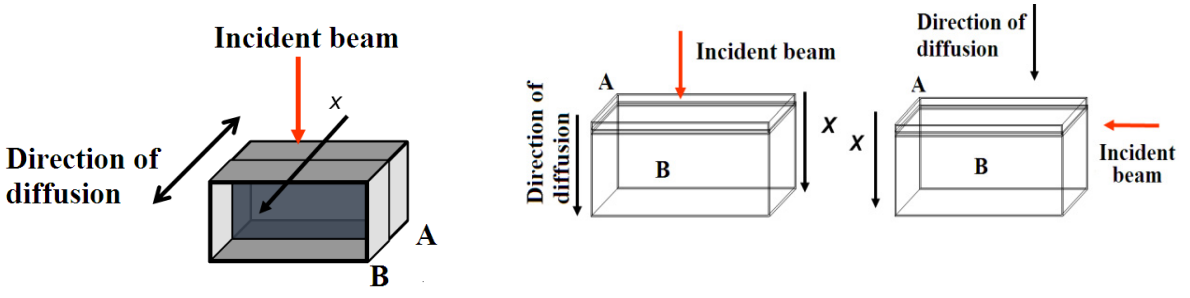

Fig. 3. Laser beam incidence on the samples: (a) diffusion couple; (b) thin deposit for infinite dilution diffusion.

Table 2. Emission patterns of the elements employed for analysis the Zr-2.5Nb/ ASTM 410 couple*

	Zr II (339)	Fe II (259-248)	Cr II (276)	Nb II (316)	Ni I (361)	Si I (252)
Wavelength (nm)	339.1972	259.83692 248.63728	276.258	316.3401	361. 9391	252.4108
Electronic configuration	$4d^2(a\ ^3\mathrm{F})5s$ $4d^2(a\ ^3\mathrm{F})5p$	$3d^6(^5\mathrm{D})4s$ $3d^6(^5\mathrm{D})4p$	$3d^4(^5\mathrm{D})4s$ $3d^4(^5\mathrm{D})4p$	$4d^3(^4\mathrm{F})5s$ $4d^3(^4\mathrm{F})5p$	$3d^9(^2\mathrm{D})4s$ $3d^9(^2\mathrm{D})4p$	$3s^23p^2$ $3s^23p4s$

* NIST Atomic Spectra Data Base (www.nist.gov/pml/data/handbook/index.cfm).

3. Results and discussion

3.1. Microstructural analysis of the interdiffusion zone in Zr-2.5Nb / ASTM 410 system

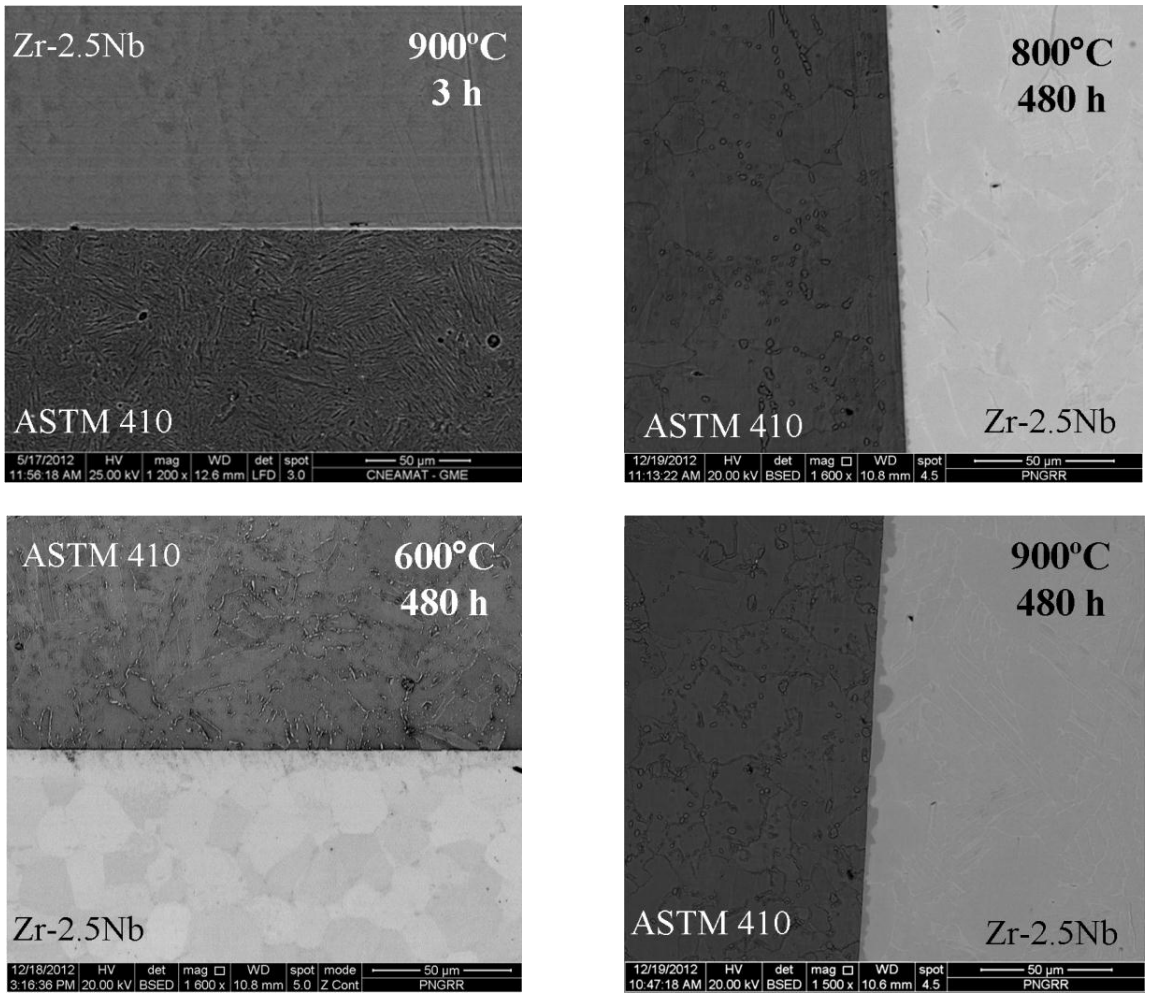

Fig. 4. Microstructural diffusion couples in Zr-2.5Nb / ASTM 410 system.

Fig. 4 shows SEM images of the microstructure of the sample heat treated at 900 °C for 3 h (adhesion heat treatment), and at 600, 800 and 900 °C for 483 h. At 600 °C the Zr-2.5Nb alloy showed equiaxial grain morphology larger than the original, attributed to the α-Zr phase growth (Figs. 5a and 5b). The sample treated at 600 °C, below the monotectoid temperature (620 °C), showed segregation of β-Nb at the triple points of the grain boundaries of the α-Zr. Relevant microstructural change in this alloy occurs between 800 and 900 °C. The images obtained by SEM shows equiaxial grains of promonotectoid α-Zr phase wholly or partially surrounded by a laminar structure of monotectoid α-Zr + β-Nb (Figs. 5d and 5c). This structure results from the treatment at 900 °C in the β-ZrNb phase field followed by slow cooling to room temperature. During the cooling, a promonotectoid α-Zr phase nucleates and grows in equilibrium with the β-ZrNb phase. During the cooling this phase is enriched in Nb until the monotectoid Nb composition (~20 wt% Nb) and it then decomposes to sheets of α-Zr + β-Nb biphasic structure. Similar microstructures were observed for studies by Iribarren et al. (2001) and Kim et al. (2005).

Microstructural changes in the ASTM 410 M steel are also significant. For Fe-11.5% Cr, similar to ASTM 410 M steel, the ferritic structure (α-Fe) is predominant from room temperature to 850 °C, where it begins the two phase field α-Fe + γ-Fe. At 600, 700 and 800 °C diffusion phenomena of C and Cr along ferrite grain boundaries occur, giving rise to the formation of Cr and Fe carbides, type $M_{23}C_6$ and M_7C_3, Fig. 6 (Raghavan, 1994). In the joint area, a growth of a dark area in the direction of the array of Zr-2.5Nb can be seen, although this effect is lower for 600 and 700 °C. At 800 and 900 °C, this area can be seen with SEM (backscattered electrons). Fig.7 shows the formation of the dark area and their growth to Zr-Nb alloy. By means of Zr-Cr and Zr-Fe diagrams the dark phase can be identified as $Zr(M)_2$ (Fd3m type), where M is a Fe and Cr atomic mixture in the junction area. The coarsening of the grains in that area is attributed to α-Zr growth exclusively.

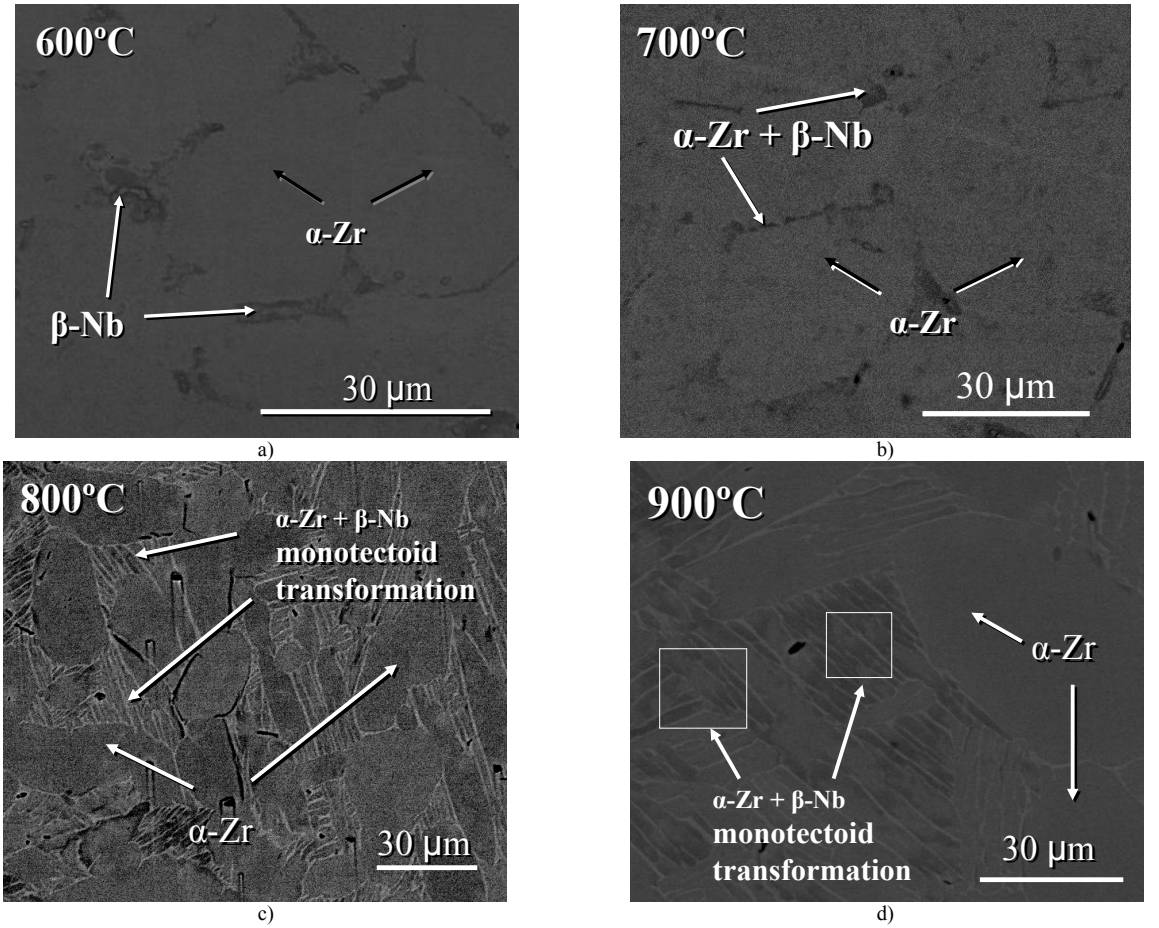

Fig. 5. Grain microstructure of the alloy Zr-2.5Nb at different temperatures.

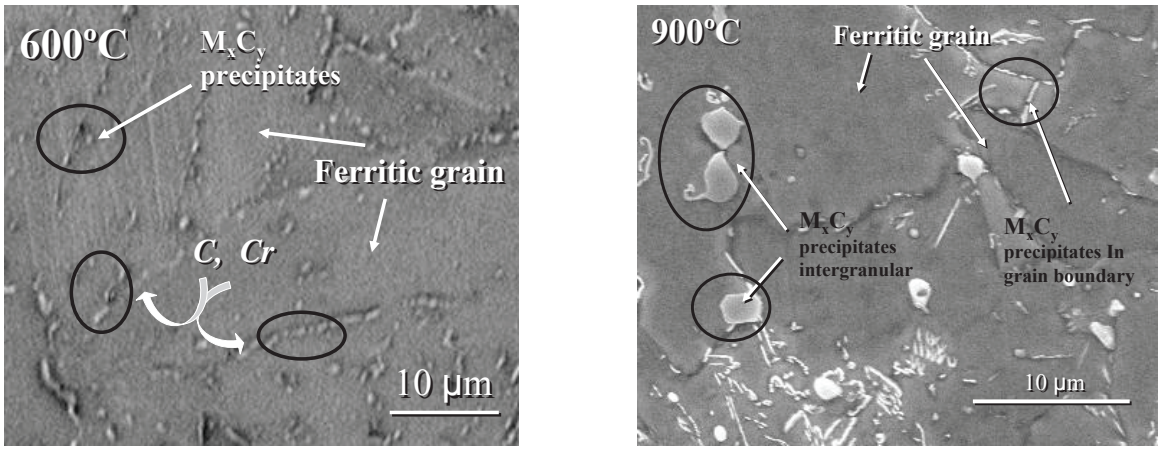

Fig. 6. ASTM 410 stainless steel heat treated at 600 to 900 ° C during 480 h.

These microstructural observations are consistent with a previous work of Bhanumurthy et al. (2001). They propose that the low growth of β-Nb phase in the grain boundaries as seen in this work, is due to the presence of dissolved oxygen in both matrices, particularly in Zr-2.5Nb. According to the Zr-O phase diagram (Massalski, 1990), the presence of oxygen (> 0.1 wt%) in the system acts as an α-Zr phase stabilizer, increasing the temperature of the transformation α+β → β-ZrNb (860 °C, according to the Zr-Nb phase diagram). Consequently, a partial transformation from α-Zr at the interface happens when the pair is heated from 800 to 900 °C, as observed in Fig. 7.

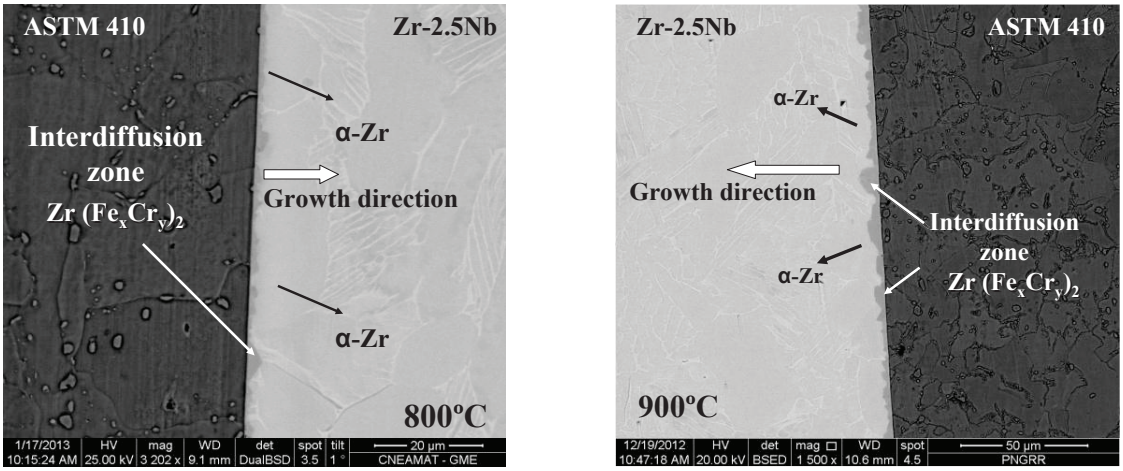

Fig. 7. SEM images of the interdiffusion zone in a diffusion couple of Zr-2.5Nb / ASTM 410 M at 800 and 900 °C during 483 h.

3.2. Obtaining of diffusion profiles for LIBS

Fig. 8a shows the sequence of LIBS emission spectra for the diffusion couples Zr-2.5Nb / ASTM 410 with an annealing of 900 °C for 19 h. The behavior of each of the present species can be seen in Fig. 8b. For this picture both the intensity of the selected emission lines, Table 2, and the advancing step in the measurement processes were considered.

For a fixed temperature (900 °C), time dependence (3, 123, 483 h) can be seen in Fig. 9 for the main elements (Fe, Zr, Cr and Nb). These graphs show that the steel elements Fe and Cr have a greater diffusion in the Zr-2.5Nb matrix than Zr and Nb in the ASTM 410 matrix.

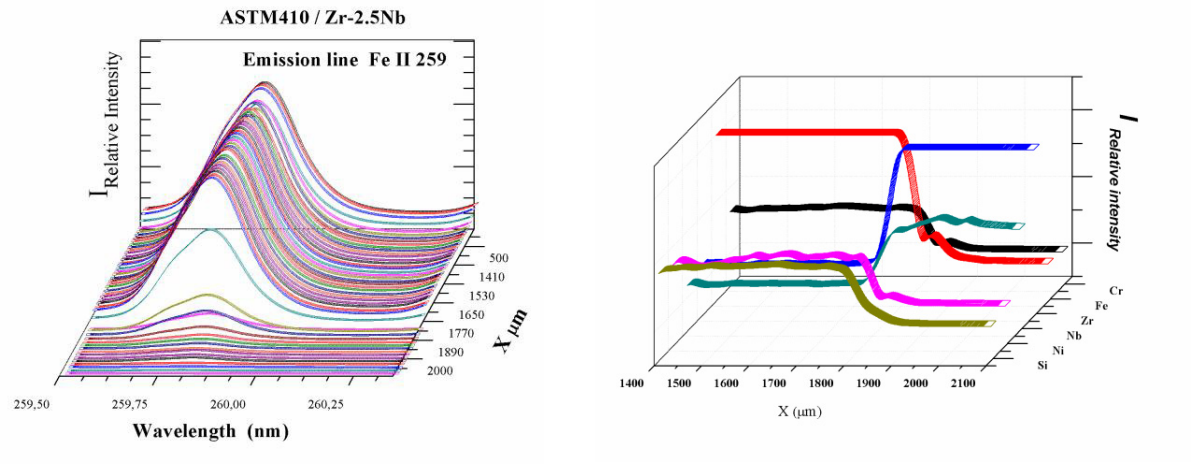

a) b)

Fig. 8. (a) Serial spectra in Zr-2.5Nb / ASTM 410; (b) Interdiffusion profile of Si, Fe, Cr, Nb, Zr and Ni .

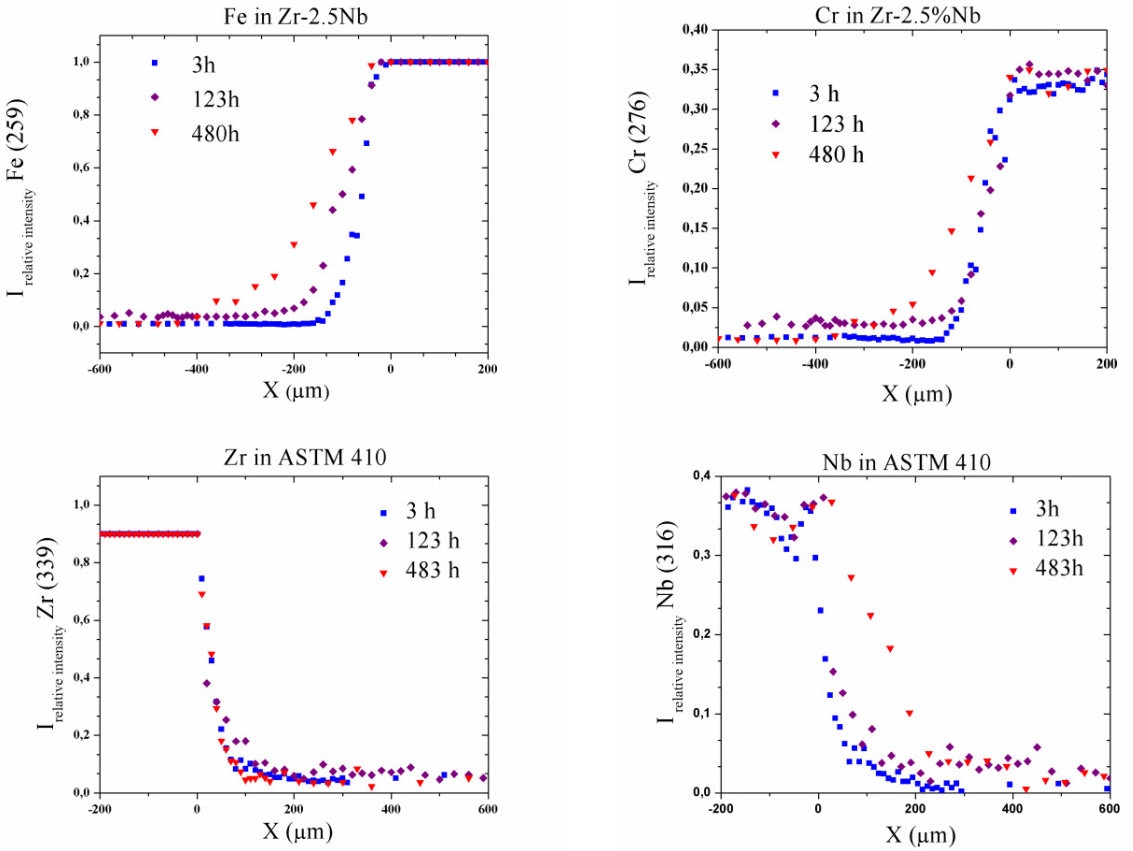

Fig. 9. Diffusion profiles of Fe, Cr, Nb and Zr on the couples Zr-2.5Nb / ASTM 410 at 900 ° C during 3, 123 and 483 h.

Also, interdiffusion profiles of the main elements obtained at different temperatures (600, 700, 800 and 900 °C) for the same annealing time (483 h) can be seen in Fig. 10. As the temperature increases, diffusion of the

elements increases too. However, the size of the crater (100-200 μm) is too large to observe in Fig. 10 the dark area formed in the interdiffusion zone (Fig. 7).

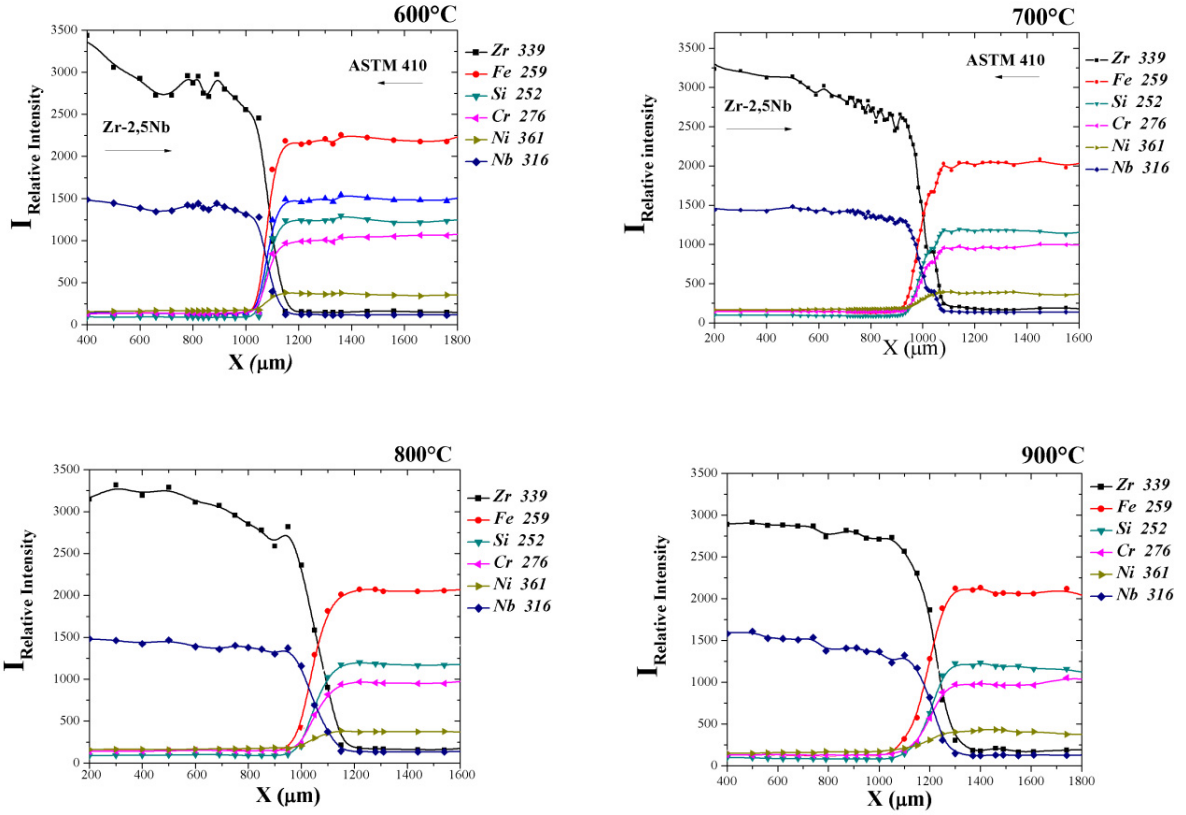

Fig. 10. Interdiffusion profiles in the Zr-2.5Nb / ASTM 410 system heat treated at different temperatures during 483 h.

3.3. Calculation of diffusion coefficients from interdiffusion profiles obtained by LIBS

The experimental determination of interdiffusion profiles were performed in a couple heat treated at 900 °C for 19 h. This temperature was selected because at 900 °C the Zr-2.5Nb alloy has a beta phase structure. This fact allows us to get an easier analysis (from a morphological point of view) of the results. To calculate the diffusion coefficients of the species, we combined the concentration curves with an error function:

$$\frac{C}{C_0} = erfc\left(\frac{x}{2\sqrt{D \cdot t}}\right) \tag{2}$$

In equation (2) we assume that the ratio of intensities equals the ratio of the concentrations ($C/C_0 \sim I/I_0$). Besides, we assume that each alloy acts as an infinite source of material. While such assumption seems to be logic, it is necessary to emphasize that the formation of intermetallic compounds (Zr, Fe and Cr) in the region adjacent to the initial interface of the Zr-based alloy do not affect the validity of the infinite source of material. This makes possible the direct application of the error function even in regions affected by slight phase reactions as the involved distances exceed largely the size of the new phases. Fig. 11 shows the graphs corresponding to the linearization of the profiles by means of the inverse of the error function. The values do not differ significantly from those reported in the literature, Table 3 (Mehrer, 1990).

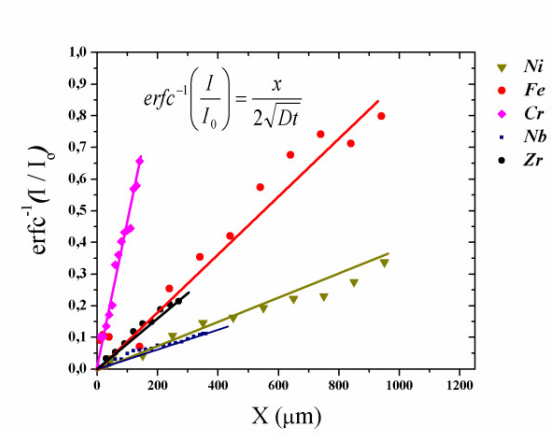

Fig. 11. Fe, Ni and Cr in Zr-2.5Nb, and Zr and Nb in ASTM 410 heat treated at 900 °C during 19 h.

Table 3. LIBS diffusion coefficients of Cr, Ni and Fe in Zr-2.5Nb and Zr and Nb in ASTM 410 at 900 °C – 19 h.

	LIBS diffusion coefficient (m^2/s)	Diffusion coefficient in pure Zr (m^2/s)**
Cr	$(1.6\pm0.5)\ 10^{-13}$	$5.5\ 10^{-14}$
Ni	$(3.8\pm0.3)\ 10^{-11}$	$4.5\ 10^{-12}$
Fe	$(4.8\pm0.6)\ 10^{-12}$	$1.1\ 10^{-12}$
Zr	$(5.8\pm0.5)\ 10^{-13}$	---
Nb	$(5.3\pm0.5)\ 10^{-12}$	---

**Reference values were taken from experiments in pure β-Zr.

3.4. Fe and Cr diffusion coefficients for infinite dilution experiment.

In order to obtain more accurate values of the migration rates of the different species, we performed diffusion experiences at infinite dilution for Fe and Cr in the matrix of Zr-2.5Nb (β phase). The experimental details were exposed in previous paragraphs and Fig. 12 shows the diffusion profiles obtained. In this case, a Gaussian solution is assumed, so,

$$\frac{C}{C_o}=\exp\left(-\frac{x^2}{4\cdot D\cdot t}\right) \tag{3}$$

Given that($C/C \sim I/I_0$), finally, we obtain the well known relation:

$$ln\left(\frac{I}{I_0}\right)=-\frac{x^2}{4Dt} \tag{4}$$

Table 4 shows the diffusion coefficient values obtained by the experiments of interdiffusion (calculated by linear regression of the error function) and the diffusion experiment at infinite dilution (calculated by regression of the Gaussian function) of Fe and Cr as well as reported literature values (Mehrer, 1990). In all cases, and by considering the use of a LIBS technique, a good agreement is achieved.

Table 4.Cr and Fe diffusion coefficients (D) obtained by LIBS inZr-2.5Nb at 900 °C.

Element	*D*(error function)(m^2/s)	*D*(Gaussian function) (m^2/s)	Diffusion coefficient in pure Zr (m^2/s)**
Cr	$(1.6\pm0.5)\ 10^{-13}$	$(2.3\pm0.5)\ 10^{-14}$	$5.5\ 10^{-13}$
Fe	$(5.8\pm0.5)\ 10^{-12}$	$(1.1\pm0.5)\ 10^{-11}$	$1.1\ 10^{-12}$

**Reference values were taken from experiments in pureβ- Zr experiments.

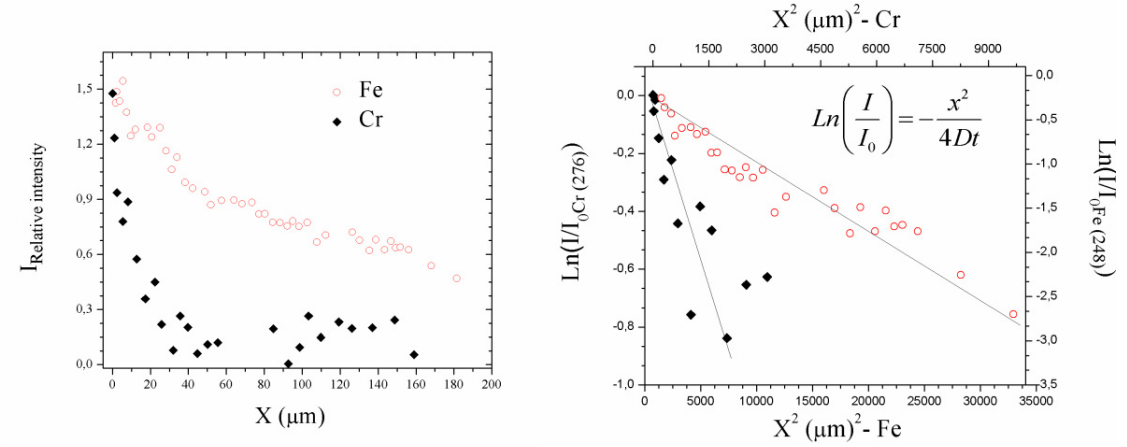

Fig. 12. (a) Fe and Cr profiles at infinite dilution experiment in Zr-2.5Nb; (b) Linear regression of Gaussian function.

4. Conclusions

- It was possible to adapt LIBS for solid state diffusion measurements in: a) interdiffusion profiles for all species diffusing simultaneously at different times and temperatures in the couple Zr-2.5Nb / ASTM 410 martensitic grade stainless steel, and b) infinite dilution diffusion measurements for Fe and Cr at 900 °C, allowing us to obtain quantitative values of the diffusion coefficient in the β-phase of Zr-2.5Nb, in very good agreement with the literature data. Although it is possible to find few diffusion studies at infinite dilution conditions, the present results can be considered as the first ones obtained in nuclear alloys by means of this technique.
- The region examined by each of the spots produced by the laser ablation is significantly large compared to the size of the growing new phases and precipitates. So the analysis was made by a complementary technique: SEM. It allowed us the identification of them, such as carbides formed by Cr and Fe in the steel. The diffusion of Fe, Cr, Ni and C in Zr-2.5Nb was much higher than the diffusion of Zr and Nb in the ASTM 410 steel matrix. So, new phases were found only in the Zr-2.5Nb matrix, while no changes were detected in the steel.
- The diffusion coefficients of Fe and Cr obtained at 900 °C are in good agreement with the literature values.

References

Ararat-Ibarguen C., 2013. *Study of interdiffusion between Zr-based alloys and nuclear stainless steels by LIBS technique*. Thesis of Master in Materials Science and Technology, Sabato Institute, National University of San Martin, Buenos Aires. 41-45.

ASTM B353-02, Standard Specification for *Wrought Zirconium and Zirconium Alloy Seamless and Welded Tubes for Nuclear Service (Except Nuclear Fuel Cladding)*.

Bhanumurthy, K., Patil, R.V., Srivatsava, D., Gawde, P.S., Kale, G.B., 2001. *Diffusion reaction between Zr-2.5 wt% Nb alloy and martensitic grade 403 stainless steel.* Journal of Nuclear Materials 297, 220-229.

Iribarren, M., Iglesias, M., Dyment, F., 2001. *Difusión de Cr en las interfases α/β de una aleación Zr-2,5% Nb.* Actas Jornadas SAM-CONAMET, 279-286.

Kim, H.G., Park, J.Y., Jong, Y.H., 2005. *Phase boundary of the Zr-rich region in commercial grade Zr-Nb alloys.* Journal of Nuclear Materials 347, 140-150.

Lee, C.G., Youn, K.T., Lee, Y., Yoo, D.S., Shimozaki, T., 2001. *Volume and Grain Boundary Diffusion of Al in β-Ti by Laser Induced Breakdown Spectrometry (LIBS)*. Defect and Diffusion Forum 194-199, 79-84.

Massalski, T.B., 1990. *Binary Alloy Phase Diagrams*, 2nd ed., ASM, Metals Park, OH.

Mehrer, H., 1990. *Landolt-Börnstein*, *Numerical Data and Functional Relationships in Science and Technology*, Vol. 26: *Diffusion and Solid Metals and Alloys*. Springer-Verlag, Berlin, 105-112.

Metals Handbook, 1985, 9th ed., Vol. 9: *Metallography and Microstructures*, ASM, Materials Park, Ohio, 280-282, 292.

Mizlolek, A., Palleschi, V., Schechter, I., 2008. *Laser-Induced Breakdown Spectrometry: Fundaments and Applications*. Cambridge University Press, Cambridge, UK.

NIST Electronic Database: www.nist.gov/pml/data/handbook/index.cfm. November 2012.

Raghavan, V., 1994. *C-Cr-Fe (Carbon-Chromium-Iron)*. Journal of Phase Equilibria 15, 418-419